ACS APPLIED MATERIALS & INTERFACES

www.acsami.org

Research Article

Printed and Laser-Activated Liquid Metal-Elastomer Conductors Enabled by Ethanol/PDMS/Liquid Metal Double Emulsions

Shanliangzi Liu, Sang Yup Kim, Kristen E. Henry, Dylan S. Shah, and Rebecca Kramer-Bottiglio*

Cite This: *ACS Appl. Mater. Interfaces* 2021, 13, 28729–28736

Read Online

ACCESS | Metrics & More | Article Recommendations | Supporting Information

ABSTRACT: Soft electronic systems require stretchable, printable conductors for applications in soft robotics, wearable technologies, and human–machine interfaces. Gallium-based room-temperature liquid metals (LMs) have emerged as promising candidates, and recent liquid metal-embedded elastomers (LMEEs) have demonstrated favorable properties such as stable conductivity during strain, cyclic durability, and patternability. Here, we present an ethanol/polydimethylsiloxane/liquid metal (EtOH/PDMS/LM) double emulsion ink that enables a fast, scalable method to print LM conductors with high conductivity (7.7×10^5 S m^{-1}), small resistance change when strained, and consistent cyclic performance (over 10,000 cycles). EtOH, the carrier solvent, is leveraged for its low viscosity to print the ink onto silicone substrates. PDMS resides at the EtOH/LM interface and cures upon deposition and EtOH evaporation, consequently bonding the LM particles to each other and to the silicone substrate. The printed PDMS–LM composite can be subsequently activated by direct laser writing, forming high-resolution electrically conductive pathways. We demonstrate the utility of the double emulsion ink by creating intricate electrical interconnects for stretchable electronic circuits. This work combines the speed, consistency, and precision of laser-assisted manufacturing with the printability, high conductivity, strain insensitivity, and mechanical robustness of the PDMS–LM composite, unlocking high-yield, high-throughput, and high-density stretchable electronics.

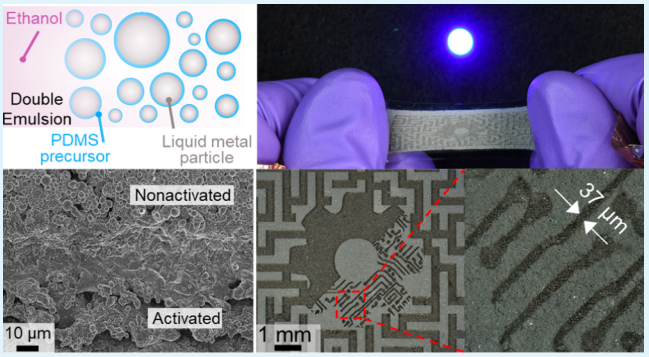

KEYWORDS: *stretchable electronics, liquid metal, double emulsion, laser sintering, liquid metal-embedded elastomer*

INTRODUCTION

Stretchable electronic systems including sensors,[1,2] electroluminescent devices,[3] energy storage devices,[4,5] and integrated circuits[6] are essential for next-generation soft robots,[7,8] wearable technologies,[9,10] and human–machine interfaces.[11,12] Stretchable materials that can maintain high conductivity as well as stable electrical and mechanical performance when strained are essential to the advancement of these soft electronic systems. Strategies to make stretchable, conductive materials include geometrical patterning of thin, rigid metal films into deterministic structures[13] as well as embedding rigid conducting/semiconducting filler materials into stretchable polymer matrices.[14] However, these materials usually suffer from low maximum strains, limited by complex structures or rigid materials.[6,14−17] Furthermore, stretching can lead to dramatic losses in electrical conductivity, limiting applications in wearable computation and soft robotics which require power and data transmission with minimal losses when strained.

Over the last decade, gallium-based room-temperature liquid metal (LM) alloys (EGaIn: 75.5% Ga/24.5% In; Galinstan: 68.5% Ga/21.5% In/10.0% Sn) have gained traction as a favorable material for stretchable electronics due to their high electrical conductivity (3.4×10^6 S · m^{-1})[18] and intrinsic stretchablity. LM alloys spontaneously form a thin passivating oxide skin (primarily Ga_2O_3) that allows them to be patterned into nonspherical shapes and encourages adhesion to surfaces.[19−21] Emerging approaches for patterning LMs include injection into microchannels,[22] lithography,[23,24] direct writing,[25] and laser ablation.[26]

For many applications, significant changes in interconnect resistance could affect signal transmission and complicate circuit design. Seeking improved electromechanical performance under strain,[27−30] recent studies have introduced liquid metal-embedded elastomer (LMEE) composites manufactured by shear mixing of the LM into a silicone matrix.[31−35] The elastomer walls surrounding the LM prevent conductivity as cast, requiring the materials to be mechanically activated to rupture the walls and form continuous electrically conductive pathways. While the meandering conductive pathways attained

Received: December 30, 2020
Accepted: May 31, 2021
Published: June 14, 2021

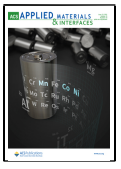

https://doi.org/10.1021/acsami.0c23108
ACS Appl. Mater. Interfaces 2021, 13, 28729–28736

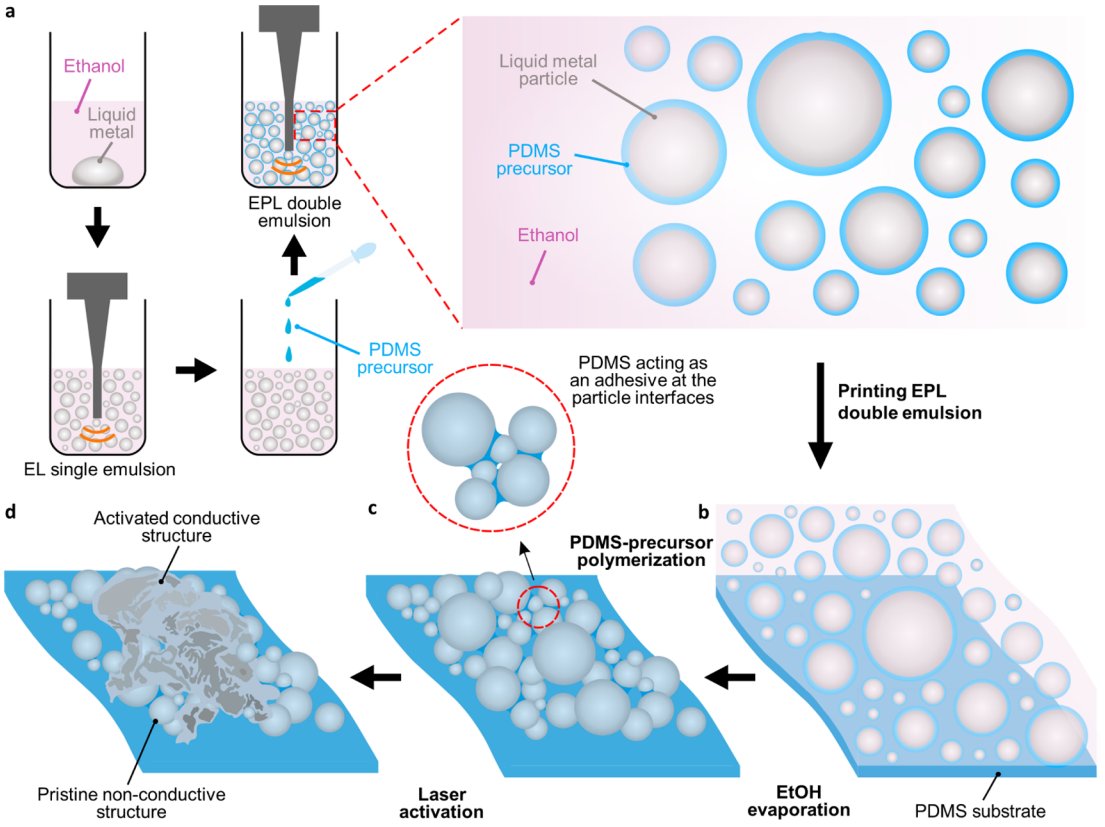

Figure 1. Illustration of the fabrication process of EPL double emulsion and PDMS−LM composite. (a) A two-step ultrasonication process creates EPL double emulsion. The double emulsion consists of LM microparticles coated by PDMS precursors in an EtOH medium. (b,c) Printing the EPL double emulsion onto a PDMS substrate creates a thin nonconductive composite material following EtOH evaporation and PDMS-precursor polymerization. The PDMS precursors reside primarily at the interfaces between the LM particles (inset), acting as an adhesive. (d) Laser activation coalesces the pristine, nonconductive structure into a continuously conductive, complex network.

by mechanical sintering in LMEEs yield a low resistance change during stretching (compared to bulk conductor assumptions),[36−38] the high viscosity of the composites prevents high-resolution printing of LMEEs. Heavy particles may also settle during the prolonged curing process, leading to nonuniform particle distribution throughout the thickness. Additionally, neighboring traces may be inadvertently connected during use due to natural mechanical sintering from handling or rapid stretching. Prior efforts to enhance processability and stability of LMEE composites include a reduction in LM loading (i.e., increasing silicone concentration[31−35]), often leading to low conductivity, slow cure times, and poor shape retention.

To enable printability of LMEE composites, we look to our prior results wherein bulk LM was made printable via emulsion processing and then sintered, either mechanically or via laser, to enable conductivity of the printed traces. Prior work demonstrated that creating an EtOH/LM (EL) single emulsion by sonicating bulk LM in ethanol, spray printing the single emulsion, and sintering the resulting LM particles on a substrate can produce thin, uniform LM films with high conductivity.[39,40] Further, laser sintering of LM particles has been shown to be fast and scalable, relative to mechanical sintering.[39−41] Yet, previous laser-sintered LM particle films were both highly sensitive to strain and also only flexible (not stretchable).[41] A laser-activated conductive trace experiences low adhesion to the substrate due to unsintered particles beneath the top sintered layer, which act as a lubricant between the sintered trace and the underlying substrate, hence forming cracks and disrupting electrical pathways during stretching.[41]

In this work, we merge the processing advantages of LM emulsions with the performance advantages of LMEEs using an ethanol/polydimethylsiloxane/liquid metal (EtOH/PDMS/LM; EPL) double emulsion. Unlike previous LM−silicone mixtures, this double emulsion ink contains a high loading of LM (~98.4 wt %), but it retains low viscosity and high stability (i.e., no particle settling). EtOH, the carrier solvent, is leveraged to facilitate printing the ink onto silicone substrates to form thin, uniform LM particle films. PDMS resides at the EtOH/LM interfaces and rapidly cures upon printing and EtOH evaporation, enabling the LM particles to form strong bonds to each other and to silicone substrates. The printed PDMS−LM composite films can be easily activated to achieve high electrical conductivity (7.7×10^5 S m^{-1}) via direct laser writing, which is attributed to the small trace thicknesses and low polymer concentrations. The laser-induced conductivity, combined with the sustained adhesion of the composite to the substrate, enables excellent electrical performance and cyclic reliability as well as provides a reliable way of rapidly creating miniaturized conductive patterns. We demonstrate an intricate, high-resolution pattern of this stretchable conductor connected as a part of an electrical circuit with an LED. Our double emulsion ink opens up possibilities for achieving stretchable, high-resolution, and device-on-demand conductive pathways, which are implementable in both soft robotics and wearable health monitoring devices.

https://doi.org/10.1021/acsami.0c23108
ACS Appl. Mater. Interfaces 2021, 13, 28729−28736

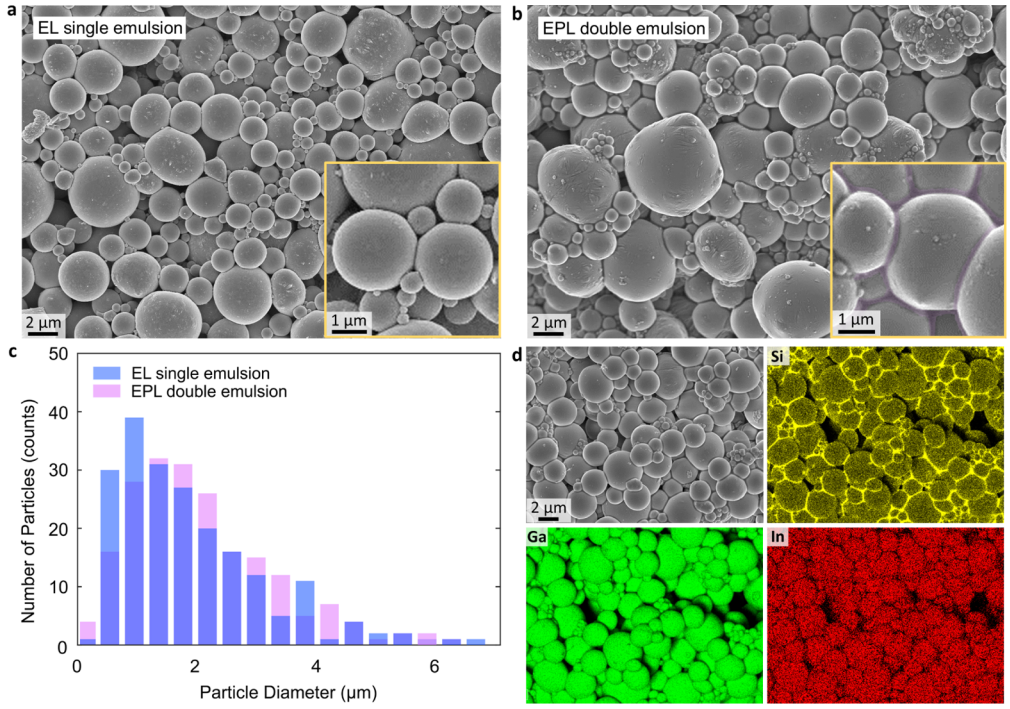

Figure 2. Material characteristics of EL single emulsion and EPL double emulsion. (a,b) SEM images of the as-printed EL single emulsion (a) and the EPL double emulsion (b). Insets are the close views showing the interfaces between the neighboring particles. The boundaries between the particles are false colored to highlight the PDMS precursors at the interfaces. (c) Histogram of particle size distributions for both the EL single emulsion (2.09 ± 1.19 μm) and the EPL double emulsion (1.91 ± 1.21 μm). (d) EDS mappings of the top surface of the as-printed EPL double emulsion, indicating higher silicon concentrations at the interfaces between the LM particles.

RESULTS AND DISCUSSION

We prepared the EPL double emulsion by first sonicating eutectic gallium−indium (eGaIn) in EtOH for 5 min, creating an EL single emulsion. Then, we removed the supernatant (small eGaIn particles dispersed in EtOH), added PDMS precursors (2−12 vol %) to the EL single emulsion, and subsequently sonicated the whole system for 3 min. Following sonication, we allowed the mixture to sit, separating out a top cream layer, with segregated PDMS precursors and lighter, noncoated LM particles from the double emulsion. We removed the cream, leaving behind the PDMS precursors, encapsulating only the larger, heavier LM particles suspended in ethanol, resulting in a EPL double emulsion (Figure 1a, Supporting Information Figure S1a). When we added an excessive amount of PDMS (>12 vol %), the PDMS precursors formed unwanted agglomerates in the EL single emulsion (Supporting Information Figure S1b). We observed the emulsion ink with 10 vol % PDMS precursors, and no agglomeration or sedimentation appeared to occur over 5 h (Supporting Information Figure S2). We also studied the rheological properties of the EPL double emulsion with 10 vol % PDMS (Supporting Information Figure S3) and found that the ink shows an apparent viscosity of 2146 Pa s at a shear rate of 0.01 s^{-1}, which is 6 orders of magnitude higher than that of pure water, but it exhibits a pronounced shear thinning behavior.

The EPL double emulsion consists of three components: (1) EtOH as the continuous phase, (2) PDMS precursors to enhance stability of the LM particles in the suspension and adhesion of the LM particles to each other and the substrate post deposition, and (3) LM enabling high electrical conductivity. In the emulsion, thin layers of liquid PDMS cover the surfaces of the LM microparticles, acting as a surfactant to stabilize the suspension in EtOH (Figure 1a). When printing onto a silicone substrate using a rod coating method (Figure 1b), EtOH evaporates rapidly, releasing the PDMS−LM droplets onto the substrate. The LM microparticles relax, and the encapsulating PDMS precursors flow and coalesce, subject to both capillary forces and gravity. The one-part PDMS precursors rapidly polymerize in contact with the atmospheric moisture and eventually cure, adhering the LM microparticles to the substrate and to each other. Upon printing, the entire curing process only takes a few minutes due to the rapid evaporation of EtOH and the small concentration of PDMS. High energy lasers can then ablate away some of the PDMS, activating the as-printed thin PDMS−LM composite (Figure 1c) into a continuously conductive, complex network (Figure 1d) that is structurally and functionally similar to previously reported LMEEs.

To study material characteristics, we compared the morphology, particle size distribution, and elemental distribution of as-printed EPL double emulsion with EL single emulsion using scanning electron microscopy (SEM) imaging and energy-dispersive X-ray spectroscopy (EDS). SEM images of the as-printed EL emulsion reveal isolated LM particles with clear, distinct boundaries (Figure 2a) and more strongly rounded shapes, while the EPL double emulsion (10 vol % PDMS) (Figure 2b) shows particles that are contiguous with each other and have blurry, noncircular boundaries between the particles (Figure 2b, boundaries false colored). This phenomenon is likely a result of the nonconductive PDMS precursors at the interfaces between the neighboring particles, accumulating electrons on the surface that deteriorates SEM image quality. The PDMS precursors, subjected to capillary forces when coalesced and cured, compress the particles into nonspherical shapes. Histograms (Figure 2c) of particle sizes show that polydispersed distributions of particle sizes for both the EL

https://doi.org/10.1021/acsami.0c23108
ACS Appl. Mater. Interfaces 2021, 13, 28729−28736

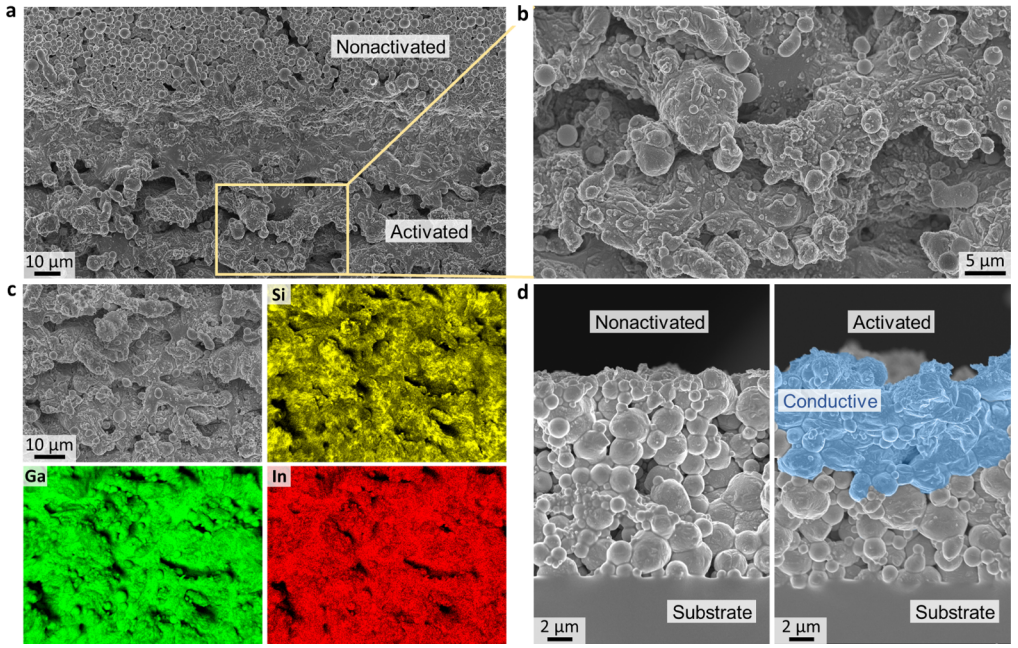

Figure 3. Laser activation of the PDMS−LM composite. (a,b) SEM images of the transition between nonactivated and activated regions of the PDMS-LM composite (a) and a detailed view of the activated, conductive region (b). (c) EDS mappings of the laser-activated PDMS−LM composite showing a uniform elemental distribution of all three key elements: Ga, In, and Si. (d) SEM images showing cross-sectional views of the PDMS−LM composite before and after laser activation. False coloring on the activated image highlights the distinct conductive, coalesced region on top.

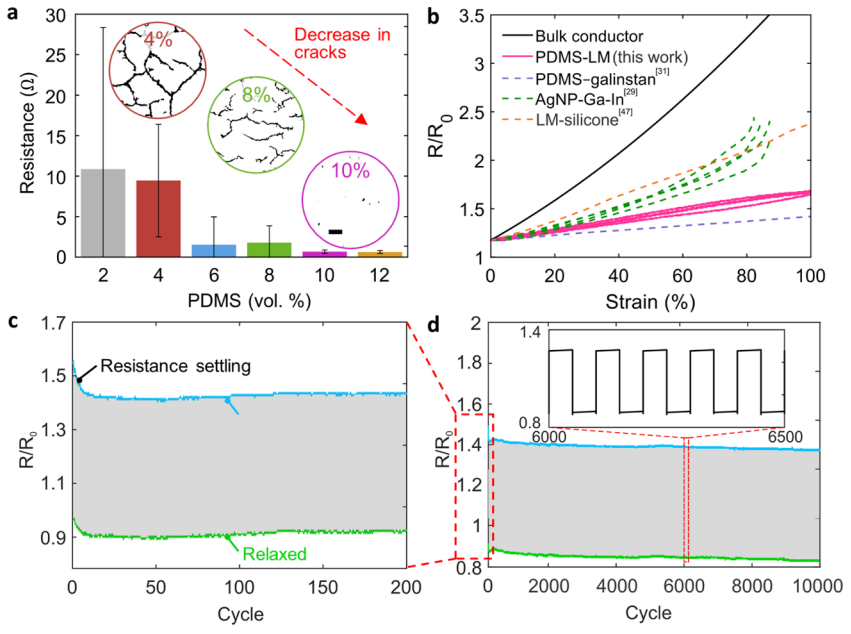

Figure 4. Electromechanical characteristics of PDMS−LM composites. (a) Resistance and surface morphology of the PDMS−LM composites at different PDMS concentrations (2−12 vol %). The composites with lower PDMS concentrations exhibit more cracks and hence larger resistance values and variances. Error bars represent 1 standard deviation. Insets are the optical images showing cracks of the PDMS−LM composite. Scale bar: 200 μm. (b) Relative change in resistance as a function of uniaxial tensile strain of the PDMS−LM composites on PDMS substrates (pink, $R/R_0 \approx 1.5 \pm 0.01$ at 100% strain, five samples), theoretical prediction based on bulk conductor assumptions (black, 3.4×10^6 S m^{-1}), and other LM-based conductors in the literature: PDMS-galinstan composite (purple),[31] AgNP−Ga−In (green),[29] and LM−silicone (orange).[47] Reproduced with permission.[31] Copyright 2015 John Wiley and Sons. Reproduced with permission.[29] Copyright 2018 John Wiley and Sons. Reproduced with permission.[47] Copyright 2015 John Wiley and Sons. (c,d), Relative resistance change of the PDMS−LM composite subjected to 10,000 cycles of 100% uniaxial tensile strain. The resistance settling during the initial 10 cycles is highlighted in (c).

single emulsion (2.09 ± 1.19 μm) and the EPL double emulsion (1.91 ± 1.21 μm) are not significantly different, so differences in particle geometry stem from a secondary influence. EDS mappings (Figure 2d) of the as-printed EPL double emulsion shows that gallium and indium are well-distributed throughout all particles, as expected, while silicon is highly concentrated at the interfaces between the LM particles. As PDMS is the only source of silicon in the EPL double emulsion, the EDS mappings

https://doi.org/10.1021/acsami.0c23108
ACS Appl. Mater. Interfaces 2021, 13, 28729−28736

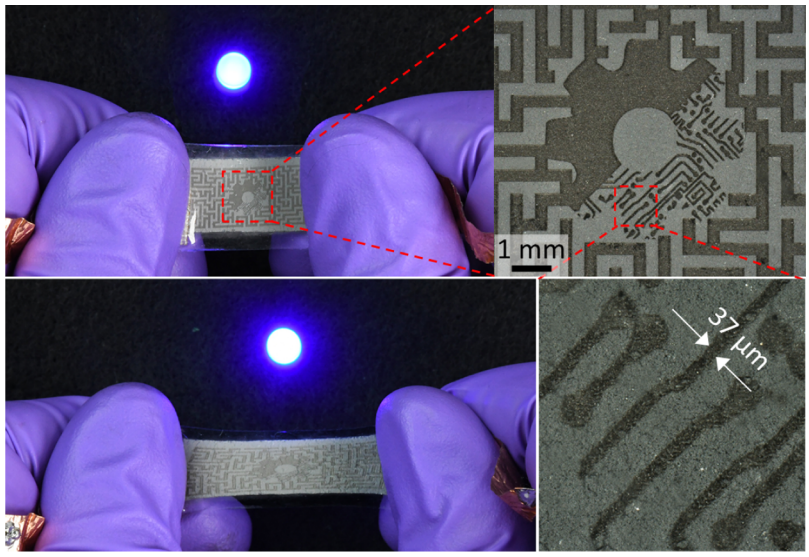

Figure 5. Demonstrations of the utility of the double emulsion ink to create stretchable electronics. Photographs of an intricate laser-activated maze pattern on a PDMS−LM composite and acting as stretchable electrical interconnects. No evident reduction of the LED brightness was observed under 80% strain. The optical microscope image shows that the single trace width created by laser activation is as small as 37 μm.

clearly demonstrate that the interparticle bridges formed by the liquid PDMS precursors (originally encasing adjacent LM particles) coalesce as EtOH evaporated.

The as-printed EPL double emulsion—which, after EtOH evaporation and PDMS coalescence, is a PDMS−LM composite—is nonconductive because the encapsulating oxide shells and now-cured PDMS layers around the LM particles both prevent spontaneous particle coalescence. We used a focused laser beam (wavelength 355 nm) to transform the nonconductive PDMS−LM composite into a conductive material (Figure 3a,b, Supporting Information Figure S4) with high electrical conductivity (7.7×10^5 S m^{-1}). The laser ablates some of the PDMS and induces large thermal stresses in the particles through rapid expansion of the LM cores.[42] The sudden expansion of the LM cores ruptures the gallium oxide shells, allowing the liquid to escape and coalesce into a continuous network.[43] Additional PDMS interfacing layers not directly ablated by the laser may also be ruptured, facilitating the formation of conductive structures. The hollow spaces (Figure 3b) within the network are presumably attributed to the vaporization of particles induced by laser ablation.[44] EDS mappings of the laser-activated PDMS−LM composite reveal silicon, gallium, and indium all well-distributed over the entire surface (Figure 3c), whereas silicone was previously isolated exclusively to the interfaces between particles. Cross-sectional SEM images of the laser-activated PDMS−LM composite (Figure 3d) show that, compared to the nonactivated PDMS−LM, the activated composite has a distinct, coalesced region on top (false colored). The PDMS acts as an adhesive, linking the top to the bottom, as evidenced by the blurry boundaries of the particles that are in contact with the underlying silicone substrate and the EDS Si mapping of the cross-sectional surface (Supporting Information Figure S5).

We varied the volume fractions of PDMS in the EPL double emulsion to investigate its role in the electrical conductivity of PDMS−LM composites (Figure 4a). The measured resistance of the composites is dependent on the PDMS concentration (2−12 vol %). Lower PDMS content in the EPL double emulsion leads to higher electrical resistance in the activated composite due to crack formation resulting from particle aggregation during EtOH evaporation (Supporting Information Figure S6).[45,46] The cracks randomly distribute throughout the composite, disrupting electrical pathways. This also caused larger variances in the measured resistance of the composites with lower PDMS content (Figure 4a). Once we increased the PDMS content to 10 vol %, the final thin-film composite became consistently uniform and crack-free on the PDMS substrate (Supporting Information Figure S7). We attribute the uniform film profile to the liquid PDMS precursors around the LM particles in the emulsion. As the EtOH evaporates, meniscus-shaped liquid PDMS bridges form between the particles, yielding capillary force that is remarkably large to overcome the gravitational forces and bring the adjacent particles together (analytical estimation in Supporting Information Figure S8). The PDMS precursors eventually cure, bonding the particles to each other and to the surfaces of the PDMS substrates. Acting as an adhesive, the PDMS precursor effectively helps alleviate the capillary pressure induced by the meniscus of the air−EtOH interface between the particles, hence preventing crack formation.[46] In addition, due to the existence of the nonconductive PDMS after laser activation, the electrical conductivity of the PDMS−LM composites is lower than that of bulk eGaIn.

To study the electromechanical performance of the PDMS−LM composite, we measured the relative resistance change (R/R_0) across a laser-activated trace as it underwent uniaxial tensile strain. The composite exhibits stable electrical performance, experiencing small resistance change on PDMS at 100% strain ($R/R_0 \approx 1.5$, Figure 4b). This value is smaller than the theoretical prediction for classical incompressible, constant-conductivity bulk conductors ($R/R_0 = (1 + \varepsilon)^2$, where ε is the applied strain; $R/R_0 = 4$ at 100% strain). Such strain-insensitive behavior has been previously reported[36] and attributed to the tortuosity of the meandering conductive pathways within LMEE composites (Figure 3b). The applied global strain largely contributes to rearrangement of the conductive pathways, still supported by intact, cross-linked PDMS, rather than changing the length or cross-sectional area of the coalesced network.

At low PDMS content, the PDMS−LM composite exhibits inconsistent and unstable electrical responses during cyclic

https://doi.org/10.1021/acsami.0c23108
ACS Appl. Mater. Interfaces 2021, 13, 28729−28736

loading (Supporting Information Figure S9). In contrast, after moderate settling during the initial cycles, the PDMS−LM composite with 10 vol % PDMS shows consistent electrical responses up to 10,000 cycles (Figure 4c,d). We suspect that the initial strain cycle ruptures the largest particles, which then consolidate into the existing conductive paths, leading to a decrease in the electrical resistance. Thereafter, the PDMS encasing the nonactivated particles bonds them to each other and to the underlying substrate, preventing crack formation (and thus loss of conductivity) and inadvertent particle coalescence that might occur during cyclic testing or other mechanical effects. In sum, the small amount of PDMS added to the initial emulsion ink creates a final conductor with favorable electrical performance and reliability.

The printable and laser-activated PDMS−LM (or LMEE) composite exhibits a superior balance of strain insensitivity, electrical conductivity, and ease of fabrication compared to other LM-based conductors in the literature (Supporting Information Table S1).[29,31,47] We demonstrate a complex maze pattern of PDMS−LM composite connected as a part of an electric circuit with a LED. We twisted, bent, and stretched the circuit to 80% strain (Figure 5a) and 50% for 100 cycles (Supporting Information Video S1), with no evident reduction of the LED brightness. The optical microscope image shows that the single conductive trace width created by laser activation is as small as 37 μm. The capability to print and laser-activate LMEEs represents an advance toward scalable manufacturing of high-density and high-performance stretchable electronics.

CONCLUSIONS

We have presented a EPL double emulsion that can be easily printed onto silicone substrates and then selectively laser-activated with intricate patterns to form stretchable conductors in a scalable fashion. EtOH, the carrier solvent, is leveraged for its low viscosity to facilitate printing. PDMS encases the LM particles in the emulsion and acts as an adhesive between the LM particles after cure, bonding the particles to each other and to silicone substrates. The strong bonding induced by the PDMS and the conductive, complex, and microporous structure induced by laser-activation enable a PDMS−LM composite with comparable behaviors to previously reported LMEEs. The composite material shows high electrical conductivity (7.7×10^5 S m^{-1}), small changes in resistance ($R/R_0 \approx 1.5$) over uniaxial tensile strains at 100%, and consistent electrical responses when stretched over 10,000 cycles. The advantageous electromechanical properties and manufacturability, combined with the prospects of generalization via different polymers and substrate materials, open up possibilities for scalable manufacturing of stretchable, multilayer, and high-density electronic circuits for various applications including soft robotics and wearables.

The ability of the material to be laser-activated illustrates the potential for this technique in making small-scale, high-density stretchable electronic circuits. In future studies, the effect of trace width on the electromechanical properties of the materials will be investigated. Additionally, it is currently unclear how the particle size and distribution affect both performance and minimum trace widths that can be reliably connected via a laser. We expect that with improved control over the particle size, distribution, and laser parameters (spot size, frequency, power, and speed), smaller trace widths and control over the path tortuosity (and therefore likely conductivity[36]) could be obtained.

EXPERIMENTAL SECTION

Preparation of EPL Double Emulsions. The EL single emulsion was created by adding 2 ± 0.02 g of eutectic gallium−indium alloy (75.5% Ga, 24.5% In, 495425, Sigma-Aldrich) into 10 mL of ethanol (V1001, Koptec) and then sonicating at an amplitude of 36 μm (30% setting) for 5 min using a tip sonicator (1/16″ microtip probe, QSonica). Following sonication, the single emulsion was stored at room temperature for an hour, allowing the heavy particles to settle under gravity. The supernatant was then removed, and the remaining heavy particle emulsion was mixed vigorously with a vortex mixer (VortexGenie) for 30 s. Two vials of the settled and vortexed emulsion were then combined and mixed again with the vortex mixer. Last, the EPL double emulsion was created by adding PDMS precursors (2−12 vol %, SEMICOSIL 964 UV/CLEAR, Wacker) into the heavy particle single emulsion and subsequently sonicating for 3 min at an amplitude of 60 μm (50% setting) pulsed for 1 s on, 1 s off. Prior to printing, the separated top layer was removed, and the double emulsion at the bottom was mixed again thoroughly with a pipette tip.

Preparation of Substrates. The substrates onto which the PDMS−LM emulsions were printed were made of PDMS (poly(dimethylsiloxane), Sylgard 184, Dow Corning). The elastomer base and the curing agent were mixed in a 10:1 ratio for 30 s and then defoamed for 30 s by the use of a planetary centrifugal mixer (ARE-310, Thinky). The PDMS was rod-coated onto a flat acrylic sheet using the approach described by White et al.[48] and cured in an incubator at 60 °C for 3 h.

Preparation of Laser-Activated PDMS−LM Composites. The EPL double emulsion was poured at one end of the cured PDMS substrate and then printed over the substrate using a custom made drawbar of 200 μm thickness. The thin composite was left at room temperature to dry and cure in a few minutes. Then, the composite was activated using an UV laser micromachining system (Protolaser U4, LPKF) with a wavelength of 355 nm, a pulse duration of 900 ns, and a beam diameter of 15 μm operated in an ambient environment. The average power used was 1.4 W with a frequency of 180 kHz and a speed of 1620 mm/s. The activated patterns were designed in CorelDraw, exported as DXF files, and then imported into the laser system software.

Electrical and Mechanical Characterization. Resistance measurements were made by laser-activating patterns with multiple connection points for performing four-terminal resistance measurements with a digital multimeter (5492B, BK Precision). The designed patterns had an aspect ratio (length/width) of 5:1 (7.5 × 1.5 mm). The values reported in Figure 4a were averaged from 10 measurements at each PDMS concentration (2−12 vol %). The measured resistance of the laser-activated PDMS−LM composite with 10 vol % PDMS was 0.68 ± 0.21 Ω and was used for conductivity calculation. Thicknesses of the laser-activated composite films were measured from Figure 3d and averaged from 10 measurements (9.69 ± 0.59 μm). The conductivity of the laser-activated PDMS−LM composite was calculated as $\sigma = l/Rwt = 7.7 \pm 0.5 \times 10^5$ S m^{-1}.

For electromechanical characterization, rectangular patterns (length: 20 mm; width: 5 mm) were lasered on the PDMS−LM composite films. Electrical connections were made by adhering copper tape on each end of the trace and then securing using silver conductive epoxy (Part# 8331-14G, MGchemicals). Fabric strips were placed at the interfaces to prevent stretching. The films were then encapsulated with PDMS. The samples were subjected to uniaxial tensile loading at 75 mm min^{-1} using a customized tensile stage. Simultaneously, the resistance was measured using a Wheatstone bridge, and the resistance of the alligator clips (0.85 Ω) was subtracted from the measurements to reduce experimental error.

Material Characterization. SEM images were taken by a Hitachi SU8230 UHR cold field emission scanning electron microscope. Samples for cross-sectional imaging were made by cleaving in liquid nitrogen. Elemental composition and mappings were obtained using EDS (Flat-Quad, Bruker) at 5 kV. Optical imaging was performed using a Zeiss Smartzoom 5 microscope. Rheological characterization was performed using a rotational rheometer (Anton Paar MCR 302) with parallel plate geometry at 20 °C (disk diameter 16 mm, gap size 1 mm).

https://doi.org/10.1021/acsami.0c23108
ACS Appl. Mater. Interfaces 2021, 13, 28729−28736

The apparent viscosity was measured at shear rates from 0.01 to 100 1/s. Strain sweep test was performed with increasing oscillation amplitude up to 500% at a frequency of 1 rad/s. Frequency sweep test (0.01−100 rad/s) was performed at 0.5% strain.

Fabrication of Stretchable Circuit Demonstrations. Patterns were designed and then imported into the laser system software. After laser activation, electrical connections were made with copper tapes and connected to an LED using biphasic gallium−indium to make reliable interfaces.[49] The circuit was encapsulated by pouring liquid PDMS over the top surface (PDMS, Sylgard 184, Dow Corning). With voltage held constant at 2.9 V, the circuit was stretched by hand or by using a customized tensile stage at 300 mm min^{-1}.

■ ASSOCIATED CONTENT

Supporting Information

The Supporting Information is available free of charge at https://pubs.acs.org/doi/10.1021/acsami.0c23108.

Circuit twisted, bent, and stretched to 80% strain and 50% strain with no evident reduction of the LED brightness (MP4)

Optical images of EtOH/PDMS/LM double emulsion with 10 and 14 vol % of PDMS precursors; optical images of EPL double emulsion with 10 vol % PDMS precursors before and after 5 h; rheological properties of EPL double emulsion with 10 vol % PDMS; optical image of a PDMS−LM composite film; EDS Si mapping of the cross-sectional surface of a laser-activated PDMS−LM composite; optical images of an as-printed EPL double emulsion with different PDMS contents; optical image of an as-printed EPL double emulsion with 10 vol % PDMS precursors; analytical estimation of the capillary force; relative resistance change of the laser-activated PDMS−LM composites with different PDMS contents subjected to uniaxial tensile cyclic loading to 100%; and electrical conductivity and relative resistance change over strain of the PDMS−LM composite and other LM-based conductors in the literature (PDF)

■ AUTHOR INFORMATION

Corresponding Author

Rebecca Kramer-Bottiglio − *School of Engineering and Applied Science, Yale University, New Haven, Connecticut 06520, United States*; Email: rebecca.kramer@yale.edu

Authors

Shanliangzi Liu − *School of Mechanical Engineering, Purdue University, West Lafayette, Indiana 47907, United States; School of Engineering and Applied Science, Yale University, New Haven, Connecticut 06520, United States*; orcid.org/0000-0002-6362-801X

Sang Yup Kim − *School of Engineering and Applied Science, Yale University, New Haven, Connecticut 06520, United States*

Kristen E. Henry − *School of Engineering and Applied Science, Yale University, New Haven, Connecticut 06520, United States*

Dylan S. Shah − *School of Engineering and Applied Science, Yale University, New Haven, Connecticut 06520, United States*

Complete contact information is available at: https://pubs.acs.org/10.1021/acsami.0c23108

Notes

The authors declare no competing financial interest.

■ ACKNOWLEDGMENTS

The authors thank Dr. Lina Sanchez Botero for performing rheology tests and related data analysis and Dr. R. Adam Bilodeau and Dr. Michelle C. Yuen for their valuable comments on the manuscript. This material is based upon work supported by the National Science Foundation under grant no. (CMMI-1812948). D.S.S. was supported by a NASA Space Technology Research Fellowship (80NSSC17K0164).

■ REFERENCES

(1) Amjadi, M.; Kyung, K.-U.; Park, I.; Sitti, M. Stretchable, Skin-mountable, and Wearable Strain Sensors and Their Potential Applications: A Review. *Adv. Funct. Mater.* **2016**, *26*, 1678−1698.

(2) Chen, D.; Pei, Q. Electronic Muscles and Skins: A Review of Soft Sensors and Actuators. *Chem. Rev.* **2017**, *117*, 11239−11268.

(3) Wang, J.; Lee, P. S. Progress and Prospects in Stretchable Electroluminescent Devices. *Nanophotonics* **2017**, *6*, 435−451.

(4) Yan, C.; Lee, P. S. Stretchable Energy Storage and Conversion Devices. *Small* **2014**, *10*, 3443−3460.

(5) Liu, W.; Song, M.-S.; Kong, B.; Cui, Y. Flexible and Stretchable Energy Storage: Recent Advances and Future Perspectives. *Adv. Mater.* **2017**, *29*, 1603436.

(6) Huang, Z.; et al. Three-Dimensional Integrated Stretchable Electronics. *Nat. Electron.* **2018**, *1*, 473−480.

(7) Wang, H.; Totaro, M.; Beccai, L. Toward Perceptive Soft Robots: Progress and Challenges. *Adv. Sci.* **2018**, *5*, 1800541.

(8) Rich, S. I.; Wood, R. J.; Majidi, C. Untethered Soft Robotics. *Nat. Electron.* **2018**, *1*, 102−112.

(9) Stoppa, M.; Chiolerio, A. Wearable Electronics and Smart Textiles: A Critical Review. *Sensors* **2014**, *14*, 11957−11992.

(10) Liu, Y.; Pharr, M.; Salvatore, G. A. Lab-on-Skin: A Review of Flexible and Stretchable Electronics for Wearable Health Monitoring. *ACS Nano* **2017**, *11*, 9614−9635.

(11) Jeong, J.-W.; Yeo, W.-H.; Akhtar, A.; Norton, J. J. S.; Kwack, Y.-J.; Li, S.; Jung, S.-Y.; Su, Y.; Lee, W.; Xia, J.; Cheng, H.; Huang, Y.; Choi, W.-S.; Bretl, T.; Rogers, J. A. Materials and Optimized Designs for Human-Machine Interfaces Via Epidermal Electronics. *Adv. Mater.* **2013**, *25*, 6839−6846.

(12) Lim, S.; Son, D.; Kim, J.; Lee, Y. B.; Song, J.-K.; Choi, S.; Lee, D. J.; Kim, J. H.; Lee, M.; Hyeon, T.; Kim, D.-H. Transparent and Stretchable Interactive Human Machine Interface Based on Patterned Graphene Heterostructures. *Adv. Funct. Mater.* **2015**, *25*, 375−383.

(13) Rogers, J. A.; Someya, T.; Huang, Y. Materials and Mechanics for Stretchable Electronics. *Science* **2010**, *327*, 1603−1607.

(14) Tee, B. C. K.; Ouyang, J. Soft Electronically Functional Polymeric Composite Materials for a Flexible and Stretchable Digital Future. *Adv. Mater.* **2018**, *30*, 1802560.

(15) Zhang, Y.; Wang, S.; Li, X.; Fan, J. A.; Xu, S.; Song, Y. M.; Choi, K.-J.; Yeo, W.-H.; Lee, W.; Nazaar, S. N.; Lu, B.; Yin, L.; Hwang, K.-C.; Rogers, J. A.; Huang, Y. Experimental and Theoretical Studies of Serpentine Microstructures Bonded To Prestrained Elastomers for Stretchable Electronics. *Adv. Funct. Mater.* **2014**, *24*, 2028−2037.

(16) Park, M.; Im, J.; Shin, M.; Min, Y.; Park, J.; Cho, H.; Park, S.; Shim, M.-B.; Jeon, S.; Chung, D.-Y.; Bae, J.; Park, J.; Jeong, U.; Kim, K. Highly Stretchable Electric Circuits from a Composite Material of Silver Nanoparticles and Elastomeric Fibres. *Nat. Nanotechnol.* **2012**, *7*, 803−809.

(17) Matsuhisa, N.; Kaltenbrunner, M.; Yokota, T.; Jinno, H.; Kuribara, K.; Sekitani, T.; Someya, T. Printable Elastic Conductors with a High Conductivity for Electronic Textile Applications. *Nat. Commun.* **2015**, *6*, 7461.

(18) Zrnić, D.; Swatik, D. S. On the Resistivity and Surface Tension of the Eutectic Alloy of Gallium and Indium. *J. Less Common. Met.* **1969**, *18*, 67−68.

(19) Dumke, M. F.; Tombrello, T. A.; Weller, R. A.; Housley, R. M.; Cirlin, E. H. Sputtering of the Gallium-Indium Eutectic Alloy in the Liquid Phase. *Surf. Sci.* **1983**, *124*, 407−422.

(20) Scharmann, F.; Cherkashinin, G.; Breternitz, V.; Knedlik, C.; Hartung, G.; Weber, T.; Schaefer, J. A. Viscosity Effect on GaInSn Studied by XPS. *Surf. Interface Anal.* **2004**, *36*, 981−985.
(21) Ladd, C.; So, J.-H.; Muth, J.; Dickey, M. D. 3D Printing of Free Standing Liquid Metal Microstructures. *Adv. Mater.* **2013**, *25*, 5081−5085.
(22) Dickey, M. D.; Chiechi, R. C.; Larsen, R. J.; Weiss, E. A.; Weitz, D. A.; Whitesides, G. M. Eutectic Gallium-Indium (EGaIn): A Liquid Metal Alloy for the Formation of Stable Structures in Microchannels at Room Temperature. *Adv. Funct. Mater.* **2008**, *18*, 1097.
(23) Kramer, R. K.; Majidi, C.; Wood, R. J. Masked Deposition of Gallium-Indium Alloys for Liquid-Embedded Elastomer Conductors. *Adv. Funct. Mater.* **2013**, *23*, 5292−5296.
(24) Gozen, B. A.; Tabatabai, A.; Ozdoganlar, O. B.; Majidi, C. High-Density Soft-Matter Electronics with Micron-Scale Line Width. *Adv. Mater.* **2014**, *26*, 5211−5216.
(25) Boley, J. W.; White, E. L.; Chiu, G. T.-C.; Kramer, R. K. Direct Writing of Gallium-Indium Alloy for Stretchable Electronics. *Adv. Funct. Mater.* **2014**, *24*, 3501−3507.
(26) Pan, C.; Kumar, K.; Li, J.; Markvicka, E. J.; Herman, P. R.; Majidi, C. Visually Imperceptible Liquid-Metal Circuits for Transparent, Stretchable Electronics with Direct Laser Writing. *Adv. Mater.* **2018**, *30*, 1706937.
(27) Zhu, S.; So, J.-H.; Mays, R.; Desai, S.; Barnes, W. R.; Pourdeyhimi, B.; Dickey, M. D. Ultrastretchable Fibers with Metallic Conductivity Using a Liquid Metal Alloy Core. *Adv. Funct. Mater.* **2013**, *23*, 2308−2314.
(28) Mengüç, Y.; Park, Y.-L.; Pei, H.; Vogt, D.; Aubin, P. M.; Winchell, E.; Fluke, L.; Stirling, L.; Wood, R. J.; Walsh, C. J. Wearable Soft Sensing Suit for Human Gait Measurement. *Int. J. Robot Res.* **2014**, *33*, 1748−1764.
(29) Tavakoli, M.; Malakooti, M. H.; Paisana, H.; Ohm, Y.; Green Marques, D.; Alhais Lopes, P.; Piedade, A. P.; de Almeida, A. T.; Majidi, C. EGaIn-Assisted Room-Temperature Sintering of Silver Nanoparticles for Stretchable, Inkjet-Printed, Thin-Film Electronics. *Adv. Mater.* **2018**, *30*, 1801852.
(30) Wang, X.; Fan, L.; Zhang, J.; Sun, X.; Chang, H.; Yuan, B.; Guo, R.; Duan, M.; Liu, J. Printed Conformable Liquid Metal e-Skin-Enabled Spatiotemporally Controlled Bioelectromagnetics for Wireless Multisite Tumor Therapy. *Adv. Funct. Mater.* **2019**, *29*, 1907063.
(31) Fassler, A.; Majidi, C. Liquid-Phase Metal Inclusions for a Conductive Polymer Composite. *Adv. Mater.* **2015**, *27*, 1928−1932.
(32) Lin, Y.; Cooper, C.; Wang, M.; Adams, J. J.; Genzer, J.; Dickey, M. D. Handwritten, Soft Circuit Boards and Antennas Using Liquid Metal Nanoparticles. *Small* **2015**, *11*, 6397−6403.
(33) Bartlett, M. D.; Kazem, N.; Powell-Palm, M. J.; Huang, X.; Sun, W.; Malen, J. A.; Majidi, C. High Thermal Conductivity in Soft Elastomers with Elongated Liquid Metal Inclusions. *Proc. Natl. Acad. Sci. U.S.A.* **2017**, *114*, 2143−2148.
(34) Markvicka, E. J.; Bartlett, M. D.; Huang, X.; Majidi, C. An Autonomously Electrically Self-Healing Liquid Metal−Elastomer Composite for Robust Soft-Matter Robotics and Electronics. *Nat. Mater.* **2018**, *17*, 618−624.
(35) Ford, M. J.; Ambulo, C. P.; Kent, T. A.; Markvicka, E. J.; Pan, C.; Malen, J.; Ware, T. H.; Majidi, C. A Multifunctional Shape-Morphing Elastomer with Liquid Metal Inclusions. *Proc. Natl. Acad. Sci. U.S.A.* **2019**, *116*, 21438−21444.
(36) Zolfaghari, N.; Khandagale, P.; Ford, M. J.; Dayal, K.; Majidi, C. Network Topologies Dictate Electromechanical Coupling in Liquid Metal−Elastomer Composites. *Soft Matter* **2020**, *16*, 8818−8825.
(37) Thrasher, C. J.; Farrell, Z. J.; Morris, N. J.; Willey, C. L.; Tabor, C. E. Mechanoresponsive Polymerized Liquid Metal Networks. *Adv. Mater.* **2019**, *31*, 1903864.
(38) Veerapandian, S.; et al. Hydrogen-Doped Viscoplastic Liquid Metal Microparticles for Stretchable Printed Metal Lines. *Nat. Mater.* **2021**, *20*, 533−540.
(39) Boley, J. W.; White, E. L.; Kramer, R. K. Mechanically Sintered Gallium-Indium Nanoparticles. *Adv. Mater.* **2015**, *27*, 2355−2360.
(40) Mohammed, M. G.; Kramer, R. All-Printed Flexible and Stretchable Electronics. *Adv. Mater.* **2017**, *29*, 1604965.
(41) Liu, S.; Yuen, M. C.; White, E. L.; Boley, J. W.; Deng, B.; Cheng, G. J.; Kramer-Bottiglio, R. Laser Sintering of Liquid Metal Nanoparticles for Scalable Manufacturing of Soft and Flexible Electronics. *ACS Appl. Mater. Interfaces* **2018**, *10*, 28232−28241.
(42) Yuen, M. C.; Kramer, R. K. Fabricating Microchannels in Elastomer Substrates for Stretchable Electronics. *International Manufacturing Science and Engineering Conference*; 2016, pp V002T01A014.
(43) Liu, S.; Reed, S. N.; Higgins, M. J.; Titus, M. S.; Kramer-Bottiglio, R. Oxide Rupture-Induced Conductivity in Liquid Metal Nanoparticles by Laser and Thermal Sintering. *Nanoscale* **2019**, *11*, 17615−17629.
(44) Lu, T.; Markvicka, E. J.; Jin, Y.; Majidi, C. Soft-Matter Printed Circuit Board with UV Laser Micropatterning. *ACS Appl. Mater. Interfaces* **2017**, *9*, 22055−22062.
(45) Jagla, E. Stable Propagation of an Ordered Array of Cracks During Directional Drying. *Phys. Rev. E: Stat., Nonlinear, Soft Matter Phys.* **2002**, *65*, 046147.
(46) Lee, W. P.; Routh, A. F. Why Do Drying Films Crack? *Langmuir* **2004**, *20*, 9885−9888.
(47) Zhou, L.-y.; Fu, J.-z.; Gao, Q.; Zhao, P.; He, Y. All-Printed Flexible and Stretchable Electronics with Pressing or Freezing Activatable Liquid-Metal−Silicone Inks. *Adv. Funct. Mater.* **2020**, *30*, 1906683.
(48) White, E. L.; Case, J. C.; Kramer, R. K. Multi-Element Strain Gauge Modules for Soft Sensory Skins. *IEEE Sensor. J.* **2015**, *16*, 2607−2616.
(49) Liu, S.; Shah, D. S.; Kramer-Bottiglio, R. Highly Stretchable Multilayer Electronic Circuits Using Biphasic Gallium-Indium. *Nat. Mater.* **2021**, *20*, 851−858.

https://doi.org/10.1021/acsami.0c23108
ACS Appl. Mater. Interfaces 2021, 13, 28729−28736